JTTEE5 18:380–391
DOI: 10.1007/s11666-009-9304-7
1059-9630/$19.00 © ASM International

Quality Improvement of Flame Sprayed, Heat Treated, and Remelted NiCrBSi Coatings

Z. Bergant and J. Grum

(Submitted September 17, 2008; in revised form December 24, 2008)

In this study, properties of NiCrBSi coatings, produced by a two-step process of flame deposition and furnace posttreatment, are analyzed. Adhesion strength, microstructure, porosity, microhardness, chemical composition, and residual stresses were analyzed after deposition and after heat treatment; that is, remelting. Numerous specimens were made to study the adhesion strength of coatings after flame deposition. The four chosen influential factors, that is, surface roughness, preheat temperature of the substrate, distance of flame torch, and type of oxyacetylene flame, were optimized to maximize the adhesion strength, using the Taguchi parametric method. The confirmation experiment showed that the developed experimental model is suitable for optimization of flame spraying deposition process. Based on the evaluation of coating properties, the best overall quality was obtained after remelting at a peak temperature 1080 °C with 5 minutes of holding time, followed by slow air cooling.

Keywords adhesion of TS coatings, hardness and (visco-) elastic properties, heat treatment of coatings, influence of spray parameters, preheating of substrates, porosity of coatings, residual stress determination

1. Introduction

The powder flame spraying method has been well known for many decades in industry. It is currently widely used for low-cost surface reparation of worn-out machine components. In the flame spray deposition process, the powder particles are partially or fully melted with an oxyacetylene flame. Particles atomize and accelerate in a turbulent flow of gases and deposit on the rough surface of a substrate, forming a coating with a lamellar and heterogeneous microstructure (Ref 1).

In the flame spraying deposition process, the most important bonding mechanism is the mechanical interlocking with the asperities of the roughened surface, in most cases made by grit or sand blasting. However, the diffusion, chemical, and physical bonds after flame deposition have a limited contribution to a higher adhesion and cohesion strength, unless the subsequent heat treatment or remelting is performed. Flame spray engineers constantly strive to attain sufficient adhesion and cohesion strength of coatings to obtain a better performance from parts (Ref 2-5). Numerous destructive methods are used to measure adhesion strength; one of the simplest is the tensile adhesive/cohesive test (TAT), standardized in ASTM C 633-01 (Ref 6). Compared to other thermal spray technologies, flame sprayed coatings show relatively limited values (Ref 1) of adhesion strength. However, flame spraying technology is still widely used, and therefore it is reasonable to examine the efficiency of modern approaches when improving the quality of coatings. The main objective of this research is to adjust the influential parameters for various combinations of the coating/substrate material to improve the adhesion strength. It is well known that the substrate preheating affects the numerous physical factors such as particle cooling rate, splat morphology, and residual stress generation during and after deposition (Ref 7-9). The final particle velocity is related to the distance from the nozzle exit to the substrate (Ref 10). The temperature field distribution of flame after nozzle is controlled with adjustment of combustion efficiency, set by oxygen-acetylene ratio, which influences the thermal energy of the particles. Grum and Slabe (Ref 11) have shown that the use of experimental methods enabled rapid optimization of processing parameters without using expensive diagnostic equipment, which is not always available in industry. The aim of the first part of the research is to optimize the flame spraying parameters using the Taguchi parametric method (Ref 12) to maximize the adhesive strength of coatings. The methodology should be also applicable for other combinations of coating/substrate where usually no subsequent heat treatment is required.

The NiCrBSi coatings are usually remelted using the flame during or after flame spraying. However, because it is difficult to control the temperature-time cycle the final through-thickness microstructure is not homogeneous. High tensile residual stress accumulation and local overheating on edges can lead to spalling or detachment of the coating from the substrate (Ref 13, 14). Many properties can be improved using furnace remelting: temperature distribution over the heated parts is more uniform, detrimental tensile residual stresses are reduced (Ref 15), the level of oxides is decreased by the deoxidation reactions in NiCrBSi coatings, pore percentage is reduced by filling

Z. Bergant and **J. Grum**, Faculty of Mechanical Engineering, University of Ljubljana, Askerceva 6, 1000 Ljubljana, Slovenia. Contact e-mails: janez.grum@fs.uni-lj.si, zoran.bergant@fs.uni-lj.si.

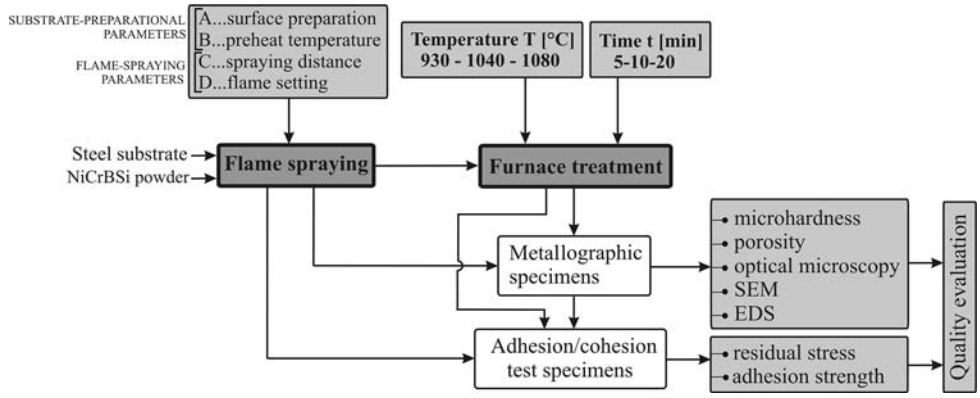

Fig. 1 Experimental procedure

Table 1 Chemical composition of NiCrBSi powder and substrate

		Composition, wt.%							
		Ni	Cr	B	Si	Fe	C	Mn	Mo
Powder	NiCrBSi	78.1	13	2.08	3.22	3.09	0.51	···	0.047
Substrate	1.0037	0.18	0.1	···	0.17	bal	0.08	0.45	···

Table 2 Parameters, codes, and level values used for Taguchi matrix experiment

Preparation and flame spray parameters	Code	Levels		
		1	2	3
Surface roughness *Ra*, μm	A	6.4	7.3	9.2
Substrate temperature, °C	B	100	150	200
Spraying distance, mm	C	150	150	200
Flame setting	D	Neutral	Carburizing	Highly carburizing

the voids with low-melting temperature eutectic phase (Ref 16, 17), the growth of hard borides and carbides increases hardness, diffusion bonding increases cohesion/adhesion strength, and so forth. In this study, the microstructural analysis is made to determine the alteration of microstructure, chemical composition, percentage of porosity, microhardness values, and residual stress for different temperature-time conditions of heat treatment, that is, remelting.

2. Experimental Design

2.1 Experimental Procedure

Figure 1 shows an experimental procedure of the two-step process: coating deposition using a flame spraying torch and coating heat treatment and remelting of the coating. The two influencing parameters of substrate surface preparation, that is, surface preparation with grit blasting and preheating of the substrate for the reduction of temperature stresses, were used. The spray process parameters chosen were the distance of the torch nozzle from the substrate surface and the mixture ratio of acetylene and oxygen. Specimens were tested for adhesion/cohesion strength, microstructure, chemical analysis, porosity, and residual stress. Additional specimens were prepared for furnace treatment. The aim of the study is to characterize the microstructure as a temperature-time dependent variable; therefore, the time-temperature conditions were changed on three levels according to a full-factorial design (Ref 18) using classical statistical methods.

In the experiment, specimen size was limited to a standard for testing adhesive strength, that is. ASTM C 633-01 (Ref 6), in which cylindrical specimens of 25 mm in diameter and 25 mm in length are coated on a face surface. The standard cylindrical specimens of the substrate were prepared from structural low-carbon steel Wr.No. 1.0037 (DIN St37.2, EN S235JR), with hardness between 200 and 240 HV. The spray device used was Rototec 80 of Castolin Eutectic (Vienna, Austria), the powder filler material was NiCrBSi with a trade name of Eutalloy 12495. An examination of powder particles with optical and electronic microscopes showed that the powder particles obtained with gas atomization were of a microspheroidal shape of the order of magnitude between 38 and 120 μm. The chemical compositions of the powder material and the substrate, taken from manufacturers' catalogs (Ref 19), are given in Table 1.

2.1.1 Surface Roughening. The substrate surfaces were prepared by grit blasting, using the three different sizes of steel grit and silicon carbide particles. The substrate is cylindrical cold-drawn steel with a diameter of 25 mm and the same length. Grit blasting was applied to one side of flat substrate surface. Preliminary tests of grit-blasting roughening were made to gradually increase the surface roughness (coded A_1, A_2, and A_3 in Table 2) of the individual specimen groups. Roughness measurements were made with a contact acicular roughness gauge Surtronic 3+, a product of Taylor/Hobson Pneumo (Taylor Hobson Ltd., Leicester, United Kingdom). The parameter used to characterize surface roughness is a mean arithmetic value of *Ra* off-size from the mean line in

a measuring length L of 8 mm with 10 measurement repetitions. The surfaces were cleaned with trichlorethylene before preheating and spraying of the coating on the surface.

2.1.2 Substrate Preheating. The preheating of the specimens was performed with an oxyacetylene flame with a Rototec 80 spraying torch (Castolin Ges.m.b.H., Vienna, Austria) to a desired temperature at levels $B_1 = 100$ °C, $B_2 = 150$ °C, and $B_3 = 200$ °C. During preheating, the specimens were mounted on a lathe drum, rotating at constant turning speed of 18 rev/min. The substrate surface temperature was measured with a contact thermocouple Ni-NiCr. The temperature was controlled manually until the desired temperature level was obtained. During flame spraying deposition of coating, the temperature of the substrate increased from an initial preheat temperature by approximately 50 °C.

2.2 Deposition of a Coating

The coating was deposited onto a flat round surface of cylindrical specimens, with diameter of 25 mm and 25 mm in length, using the Rototec 80 flame spraying torch. The specimens were mounted on the drum and a holder for the torch with constant rotation of 18 rev/min and feed 2 mm/rev (Fig. 2). During rotation, the powder flow was turned on at a position without specimens and finished after 12 passes of the torch through the specimens. The spraying distances varied, that is, $C_1 = 150$ mm, $C_2 = 175$ mm, and $C_3 = 200$ mm. The final coating thickness was measured with a micrometer at five measuring points, controlled on each specimen. With technique described, the average coating thickness of 530 μm was obtained. After remelting, the coating thickness reduced by approximately 20%.

Settings of the oxyacetylene flame at the torch were changed with an acetylene flow-rate control valve. During deposition, the operating pressure of the gases was kept constant, that is, 4 bar for oxygen and 0.7 bar for acetylene. Neutral flame of level D_1 corresponds to the flow-rate ratio of oxygen to acetylene $C_2H_2/O_2 = 1$. At this setting, the length of the core flame amounts to approximately 12 mm. Carburizing flame of level D_2 was set with a slightly higher flow of acetylene and leads to core length of approximately 15 to 20 mm. Highly carburizing flame of level D_3 was set with strong surplus of acetylene and led to a core length of 25 to 30 mm. The inner, lighter core has a temperature of approximately 3150 °C, which is significantly higher than the melting point of powder particles. When the flame is rich in acetylene, the flame core length and volume increase and therefore the degree of particle remelting increases, which is the consequence of a longer particle dwell time.

Table 2 indicates the field of investigation, which is limited by the upper and the lower limits of preparation and flame spray parameters with three factor levels. For the experiment, a three-level standard orthogonal array L_9 (3^4) was chosen, which is suitable for treatment of up to four process parameters (from A through D) at different levels. An experiment with array L_9 requires a total of nine experiments with different combinations of levels of individual parameters.

2.3 Heat Treatment and Remelting

In step 2, heat treatment and remelting of nine specimens in the furnace with a protective atmosphere was performed. In order to study effects of short-term heat treatment, three temperature and time levels between 930 and 1080 °C were chosen. The first temperature level was 930 °C, with which an overheated state of the coating at elevated temperatures was simulated; the second level was a threshold temperature of 1040 °C, at which a melt will begin to form (solidus line). When choosing the higher temperature, it is important to note that in a coating there is still a hard phase present, which hinders draining of the melt from the surface. Consequently, the highest temperature level chosen was a temperature of 1080 °C, which is below the liquidus line of NiCrBSi alloy, that is, 1110 °C. Holding times of 5, 10, and 20 min were chosen on the basis of a literature review on remelting of NiCrBSi alloy (Ref 16, 17, 19).

3. Analysis of Results

3.1 Taguchi Parametric Method and Analysis

The Taguchi method was used to optimize parameters to maximize the adhesion strength. The Taguchi parametric method belongs to modern statistical methods designed for rapid prediction of optimum process parameters (Ref 12). The Taguchi method uses the orthogonal arrays, significantly reducing the number of experiments.

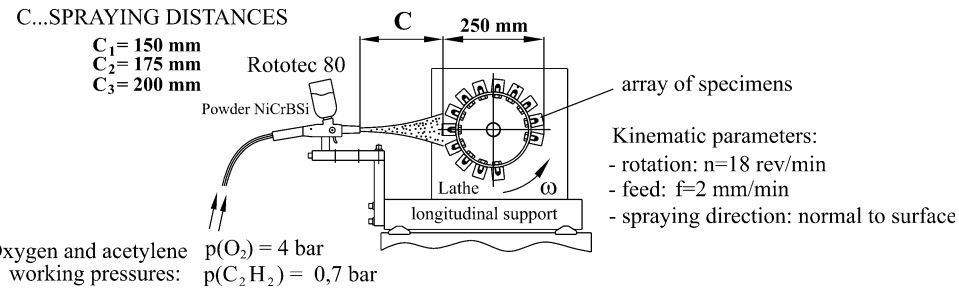

Fig. 2 Setup of experimental flame spraying deposition of coatings on specimens

The signal-to-noise (S/N) ratio is the mathematical expression for quality, and it is related to the response variable under study—adhesive strength. It should be as high as possible; therefore, the equation for S/N or η chosen is called ''the larger-the-better'':

$$\eta = -10 \cdot \log_{10}\left(\frac{1}{n}\sum_{i=1}^{n}\frac{1}{\sigma_i^2}\right) \quad \text{(Eq 1)}$$

where σ is the adhesion strength as a response variable and n is the number of experiment repetitions. In this expression there is a logarithm of an average sum of mean square reciprocal values of adhesive strength. A logarithmic transformation of the value given contributes to additivity of individual influences of factors when a prediction equation is used.

Experimental data of measured values of adhesion strength were analyzed using a 3^4 factorial design using the standard L_9 inner array. A series of 36 specimens was prepared for main matrix experiment with nine experiments with $n = 4$ repetitions. Confirmation experiment (CE) number No. 10, was performed to verify the optimum settings. Results of adhesive strength of individual experiments σ_i, an average of measurements of adhesive strength $\overline{\sigma_i}$ and S/N ratio η_i, calculated with Eq 1 are given in Table 3.

The analysis of variance is used for L_9 matrix to determine the statistical significance of the individual process parameters out of the calculated signal-to-noise ratios η. The grand total sum of squares (*GTSS*) is a sum of squared values of η:

$$GTSS = \sum_{i=1}^{9}(\eta_i)^2 \quad \text{(Eq 2)}$$

GTSS can be decomposed into two parts, sum of squares due to the mean SS_m (Eq 3) and a total sum of squares SS_T (Eq 4):

$$SS_m = \sum_{i=1}^{9}(\eta_i - m)^2 \quad \text{(Eq 3)}$$

$$SS_T = N \cdot m^2 \quad \text{(Eq 4)}$$

where N is the number of tests in matrix, and m is the mean value of the signal-to-noise ratio:

$$m = \frac{1}{9}\sum_{i=1}^{9}\eta_i = 25.08\,\text{dB} \quad \text{(Eq 5)}$$

The sum of squares of each factor (SS_m) is the relative significance on changing of η, and it is tabulated in Table 4. The parameter ''substrate temperature'' explains a major portion of the total variation of η. It is responsible for (14.25/24.24) × 100 = 59% of the variation of η. Similarly, the relative significance is calculated for other parameters. A calculation shows that the spray distance

Table 3 Array experiment with standard orthogonal array L_9 (3^4), measurement results of adhesion strength, and calculated S/N ratio η_i

	Parameter				Test repetitions $n = 4$						
Array $L_9(3^4)$	A	B	C	D	σ_1	σ_2	σ_3	σ_4	Average σ_1, (MPa)	Standard deviation S_i, MPa	Signal/noise η_i, MPa
1	1	1	1	1	10.36	11.73	11.30	11.32	*11.17*	0.58	*20.93*
2	1	2	2	2	18.76	18.8	19.03	20.05	19.16	0.61	25.63
3	1	3	3	3	19.76	20.27	20.51	21.41	20.49	0.69	26.22
4	2	1	2	3	16.06	16.20	17.07	16.50	16.46	0.45	24.32
5	2	2	3	1	21.76	19.33	20.07	21.06	20.55	1.07	26.23
6	2	3	1	2	20.39	20.45	20.02	16.73	19.40	*1.79*	25.66
7	3	1	3	2	17.68	17.37	17.01	17.09	17.29	0.30	24.75
8	3	2	1	3	18.31	18.19	17.88	18.15	18.13	0.18	25.17
9	3	3	2	1	21.70	22.92	21.45	21.95	22.01	0.64	26.85
10:CE	3	3	3	2	21.92	22.04	22.79	22.66	22.35	0.44	26.98

Note: A, surface preparations; B, substrate temperature; C, spray distance; D, flame setting; CE, confirmation experiment

Table 4 Mean values of signal-to-noise ratios η (dB) for each level and results of ANOVA

		Mean values η (dB)							
Flame spray control factors	Code	1	2	3	d.f.(a)	SS(b)	MS(c)	F ratio	%(d)
Surface roughness *Ra*, μm	A	24.26	25.40	25.59	2	3.08	1.541	3.891	12.71
Substrate temperature, °C	B	23.34	25.68	26.24	2	14.25	7.122	17.98	58.76
Spraying distance, mm	C	23.92	24.03	25.73	2	6.12	3.061	7.729	25.25
Flame setting	D	24.67	25.35	25.24	2	0.79	0.396	···	3.26
Total					8	24.24(e)	···	···	···
Error (pooled)					(2)	(0.79)	···	···	···

(a) Degrees of freedom. (b) Sum of squares. (c) Mean squares. (d) Percentage contribution of each factor. (e) Grand sum of total squares (*GTSS*)

contributes 25% of relative influence on adhesive strength, surface roughness 13%, and flame setting only 3%. The matrix experiment L_9 with nine rows has 9 degrees of freedom and so does the grand total sum of squares *GTSS*. In general, the degrees of freedom associated with a factor are 1 less than the number of levels, which is 3. Therefore, four factors A, B, C, and D have 2 degrees of freedom (3 − 1 = 2), so the total number of degrees of freedom for L_9 matrix experiment is 2 * 4 = 8.

Optimum conditions are determined out of an average of S/N ratios using a procedure called ''analysis of mean values.'' For each parameter, a mean value of the S/N ratio designated $m_{\text{factor,level}}$ is calculated. For example, an equation for the calculation of a mean value of the S/N ratio m for parameter A at the first level:

$$m_{A_1} = \frac{1}{3}(\eta_1 + \eta_2 + \eta_3) \qquad \text{(Eq 6)}$$

where η_1, η_2, and η_3 are the values of η (the first three values in column η_i, Table 3). Similarly, calculations are made for the other levels of factors A, B, C, and D. The highest values of mean for individual parameters are the optimum points A_3, B_3, C_3, and D_2, given in Table 4. The experimental error was estimated using technique ''pooling'' of the two least influential parameters, described by Phadke (Ref 12).

The trends in response graphs of signal-to-noise ratios versus parameter settings are similar to those for adhesion strength because of the low standard deviation at repetition of experiments. In such cases, it is more interesting to study the response variable, that is, adhesion strength, directly. Figure 3 shows response graphs of adhesion strength for four parameters.

For parameters A, B, and C, the increase of adhesion strength is observed when changing the level from 1 to 3. The adhesion strength increases by more than 5 MPa as the substrate temperature increases from 100 to 200 °C. Also, the adhesion strength improves by approximately 3 MPa as the spraying distance increases from 150 to 200 mm. The adhesion strength increases by more than 2 MPa as the surface roughness changes from A_1 to A_3. The optimal condition of substrate preparation and flame spraying has parameters at the highest values of adhesion strength; $A_3 = Ra = 9.2$ μm, B_3 = preheat temperature of the substrate, which is 200 °C, C_3 = spraying distance between the nozzle and the substrate surface equals 200 mm, and D_2 = setting of a flame with a slightly carbonaceous mixture.

In the partial factorial experiment L_9 experiment, nine experiments were performed under different nonoptimal combinations. However, the additional experiment must be done to confirm the optimum setting A_3, B_3, C_3, and D_2. The obtained value is then compared to the predicted value of response variable, transformed into signal-to-noise ratio, using Eq 1.

A prediction equation, that is, an additive model, is used to calculate and compare theoretically and experimentally obtained S/N ratios. The additivity of the model is an assumption that with simple addition or subtraction of deviations from the mean value of S/N ratio, m, the response (adhesion strength) under optimum conditions can be predicted. Deviations are defined as $(m_{\text{factor,level}} - m)$. The prediction equation is expressed in a general form as:

$$\eta_{\text{predicted}} = m + \sum_i m_{\text{factor,level}} - m \qquad \text{(Eq 7)}$$

where m is the mean value of the S/N ratio of the entire experiment and $m_{\text{factor,level}}$ is the mean value of individual parameters at one of the three settings. Equation 7 for the parameters (from A through D) at the optimum levels (A_3, B_3, C_3, D_2) becomes:

$$\eta_{\text{predicted}}(A_3, B_3, C_3, D_2) = m + (m_{A_3} - m) + (m_{B_3} - m) + (m_{C_3} - m) + (m_{D_2} - m) \qquad \text{(Eq 8)}$$

The calculated value of the predicted signal-to-noise ratio amounts to $\eta_{\text{predicted}} = 27.67$ dB. From the last row of Table 3, the average value of the signal-to-noise ratio from the confirmation experiment (CE), η_{opt} is 26.98 dB. The equality $\eta_{\text{predicted}} = \eta_{\text{opt}}$ is not possible because of the interactions between the parameters. Results indicate that $\eta_{\text{predicted}} > \eta_{\text{opt}}$ with the small difference (0.7 dB). Also,

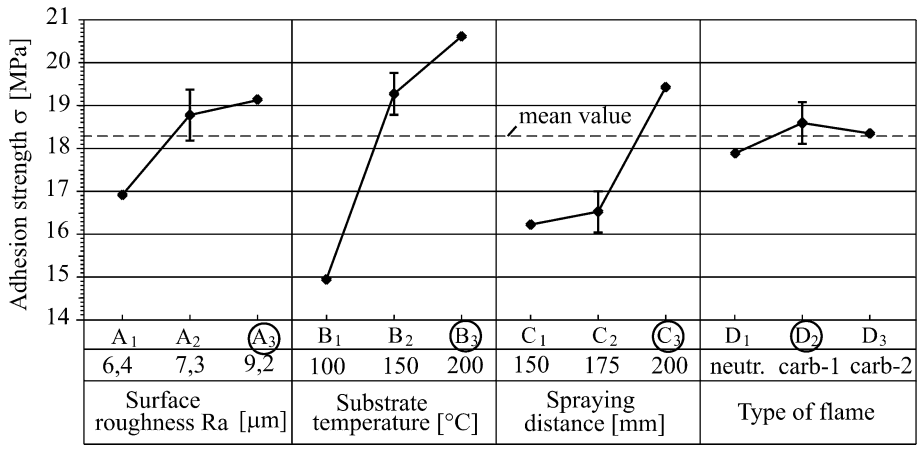

Fig. 3 Response graphs of adhesion strength for the investigated parameters

the average adhesive strength is higher than all the values obtained in the main L_9 matrix experiment. From that, we can conclude that the Taguchi parametric method is a promising technique in the optimization of the chosen parameters to maximize the adhesion strength.

3.2 Analysis of the Substrate Surface after the Tensile Adhesion/Cohesion Test

The location of failure of the adhesion/cohesion test specimens after spraying was located approximately at the interface of the coating/substrate in all the tests. Figure 4 shows residual coating material on the substrate after tensile adhesion/cohesion strength test. According to standard ASTM C 633-01 (Ref 6), the adhesion strength of coating is given if failure is entirely at the coating/substrate interface. The cohesion strength is given if rupture is only within the coating. If failure occurs in a combination of these locations in one specimen, generally no interpretations of the initial cause can be provided. The failure in experiment 1 was of the adhesive type, whereas the failures with the other specimens of experiments 2 through 9 occurred at the coating/substrate interface; a smaller fraction of the coating remained at the substrate. The fraction of the coating remnants at the substrate surface was evaluated by means of a graphical analysis based on a contrast distinction of light and dark spots in graphics (ImageTool v3.0). In experiment 1, in which the lowest measured adhesive strength amounted to 11 MPa, no coating remnants were visible at the substrate surface. In experiment 4, the value of adhesion strength measured is 16 MPa and approximately 14% of the entire surface area is covered with coating remnants. In the confirmation experiment, in which the highest average adhesive strength, that is, 22.25 MPa, was measured, a significantly larger area, approximately 54% of the entire surface area remained covered. The analysis of residuals for all specimens confirmed the increasing trend of the adhesive strength with estimated percentage of coating remnants.

3.3 Results and Analysis after Subsequent Heat Treatment and Remelting

3.3.1 Adhesion/Cohesion Strength Measurements. After heat treatment and remelting of specimens, additional tensile adhesion/cohesion tests were performed. In all cases, the failure of the glued joint occurred through the glued cross section; therefore, the values of the adhesion strength are not valid. After heat treatment, the adhesion strength of coating/interface and the cohesion of the coating are larger than the strength of the glued joint, which is approximately 50 MPa.

3.3.2 Microstructural and Microchemical Analyses of the NiCrBSi Coating. The binary phase diagrams such as NiCr, NiB, and NiSi (Ref 20) provide information about the effects of particular alloying elements on the melting temperature of a NiCrBSi system. Phase binary diagrams show that Cr, Si, and B reduce the melting temperature point of pure nickel. As a result, the melting of the eutectic phase of NiCrBSi alloy concerned (commercial name Eutalloy RW) with 13% Cr, 2.1% B, and 3.2 % Si starts at the relatively low temperature of 1040 °C. At temperature 1110 °C, the entire coating becomes liquid (Ref 19). Microstructural studies (Ref 13, 16) made on NiCrSi alloys contributed to recognizing the phases of NiCrBSi system after remelting. The matrix of the NiCrBSi alloy contains a γNi solution with a low fraction of Ni-Ni_3B eutectic with a comparatively low melting temperature. Kim et al. (Ref 17) showed that, during remelting, chromium carbide (Cr_7C_3) precipitate growth occurs in cases where the carbon content in the chemical composition of a coating exceeds 0.8 wt.%. Also, if the content of boron in the coating exceeds 2 wt.%, the microstructure contains precipitates of chromium boride (CrB).

In the preparation of the specimens for a metallographic analysis and microhardness measurements, recommendations on a standard preparation of thermal sprayed specimens in accordance with ASTM E 1920-03 were taken into account (Ref 21). The specimens were cut

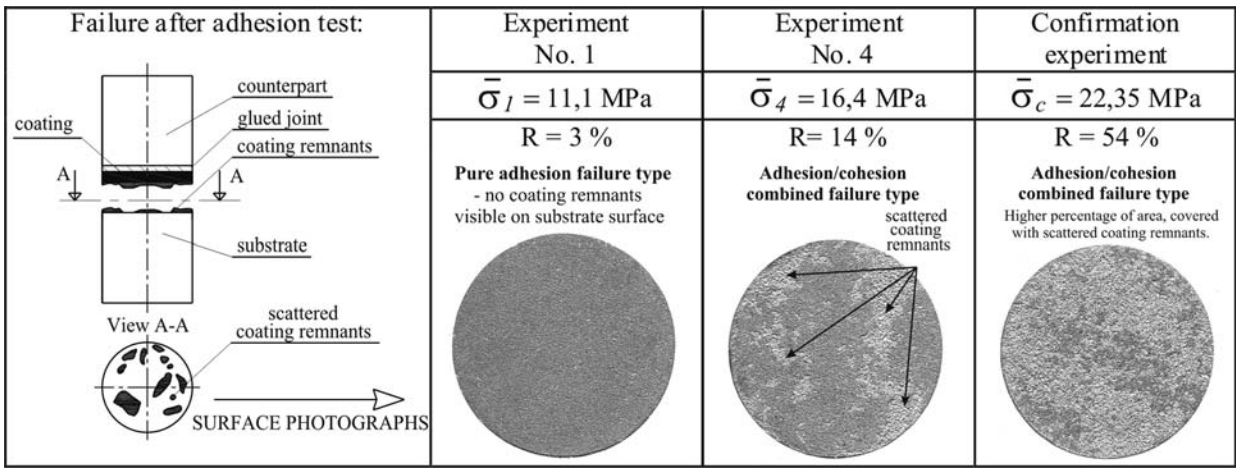

Fig. 4 Representative substrate surfaces after tensile adhesion test

in the direction running from the coating surface to the substrate, which made it possible to avoid longitudinal delamination of the coating. Grinding was carried out with a SiC paper, followed by machine polishing of the sprayed specimens with a polycrystalline diamond with grains of 3 μm, that is, 1 μm in distilled water. The specimens were inserted in a graphite powder, which provided electrical conductivity. Etching of substrate was performed with 10% nital. NiCrBSi coating was etched with a 50% HCl solution, 33% glycerol, and 16% HNO_3. The chemical analysis was carried out with JEOL JXA-8600 scanning electronic microscope (SEM, JEOL Ltd., Tokyo, Japan) with the addition of microsensor for energy-dispersive spectroscopy (EDS).With the spot and area microchemical analyses of the Ni-Cr-B-Si coating alloy six elements, that is, Ni, Cr, B, Si, Fe, and C, were detected. However, because of the microsensor detecting sensitivity limit on microprobe, the weight percentage of B_5 boron and C_6 cannot be determined, although their presence can be confirmed. Consequently, the microchemical analyses in this study were focused on sensing the fractions of four elements in the alloy, that is, nickel (Ni_{28}), chromium (Cr_{24}), silicon (Si_{14}), and iron (Fe_{26}).

Figure 5 shows gradual changes of the NiCrBSi alloy microstructure. Figure 5(a) shows a microstructure of a microspheroidal powder particle after atomization. Uniformly distributed dark gray dendritic phase A and a light matrix phase B can be distinguished. From a review of literature on microstructural changes (Ref 13, 16, 17) it can be inferred that the matrix phase B is gamma nickel (γNi) with fine-grained eutectic (Ni-Ni_3B). Figure 5(b) shows a detail of the sprayed coating with two microstructurally different particles or splats, divided by splat boundary showing poor cohesion. The upper splat was flame melted and resolidified (Fig. 5b, above), showing a fine microstructure with a nanoscale grain size. Unmelted splat (Fig. 5b, below) shows a similar microstructural texture to powder particles before spraying. Figure 5(c) shows a coating microstructure after 5 min remelting at 1080 °C. Characteristics of the remelted coating are an increased size of crystal grain of deeper-etched phase A and matrix B. Inside phase A, the small and uniformly distributed precipitates C are visible, which are richer in chromium. The selected detail in Fig. 5(c) shows a partially filled pore, that is, incomplete fusion of the liquid phase with the adjacent material.

3.3.3 Metallographic Analysis of Specimens after Heat Treatment (after Furnace Melting). Figure 6 shows micrographs of the specimens after heat treatment and remelting, that is, Fig. 6(a), (b), and (c) after heat treatment at 930 °C, Fig. 6(d), (e), and (f) after heat treatment at 1040 °C, and in Fig. 6(g), (h), and (i) after remelting at 1080 °C. All the original microstructures refer to the coating surfaces magnified 1000×.

After heat treatment at 930 °C, the microstructure formed has, in all cases regardless of the treatment time, very fine crystal grains. Boundaries among individual splats as well as surface nonflatness are clearly visible. After heat treatment at 1040 °C Fig. 6(d), (e), and (f), depending on the heat treatment time, the boundaries among the individual splats gradually disappear, but at the same time the grain size gradually increases.

For the 5, 10 and 20 min of remelting at 1080 °C, that is, between the solidus and liquidus lines of the alloy, the results of the chemical weight percentage are given in Table 5. The nickel content measured in phase A is by a 8.33 wt.% lower than the nickel content measured in phase B. As a balance, phase A is richer in chromium and silicon. Precipitates C are visible within phase A and have a higher weight percentage of chromium and are uniformly distributed after 5 min of remelting. After 10 and 20 min, remelting the number of precipitates C decreases in the surface layer, Fig. 6(h) and (i). Darker blockylike chromium-rich precipitates D were found within the phase B after remelting. The chromium content in precipitates depends on the melting time. After 5 min remelting the chromium content amounts to 56 wt.%, after 10 min melting to 84 wt.%, and after 20 min remelting to 97 wt.%. Precipitates D are most probably chromium borides CrB since the composition of the alloy concerned.

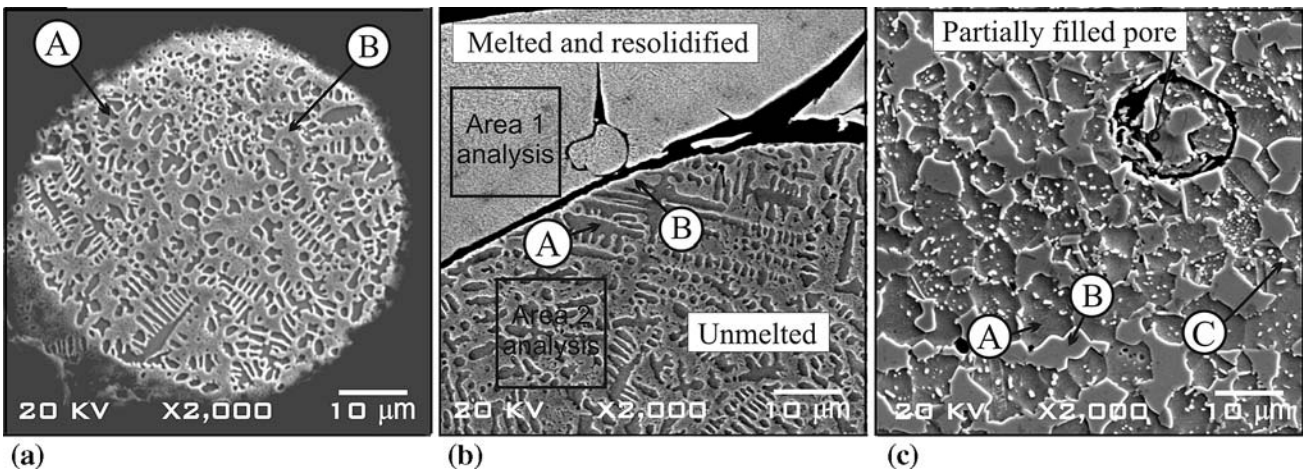

Fig. 5 Microstructural changes of NiCrBSi alloy. (a) Atomized powder NiCrBSi. (b) Coating detail after flame spraying. (c) Remelted at 1080 °C, 5 min

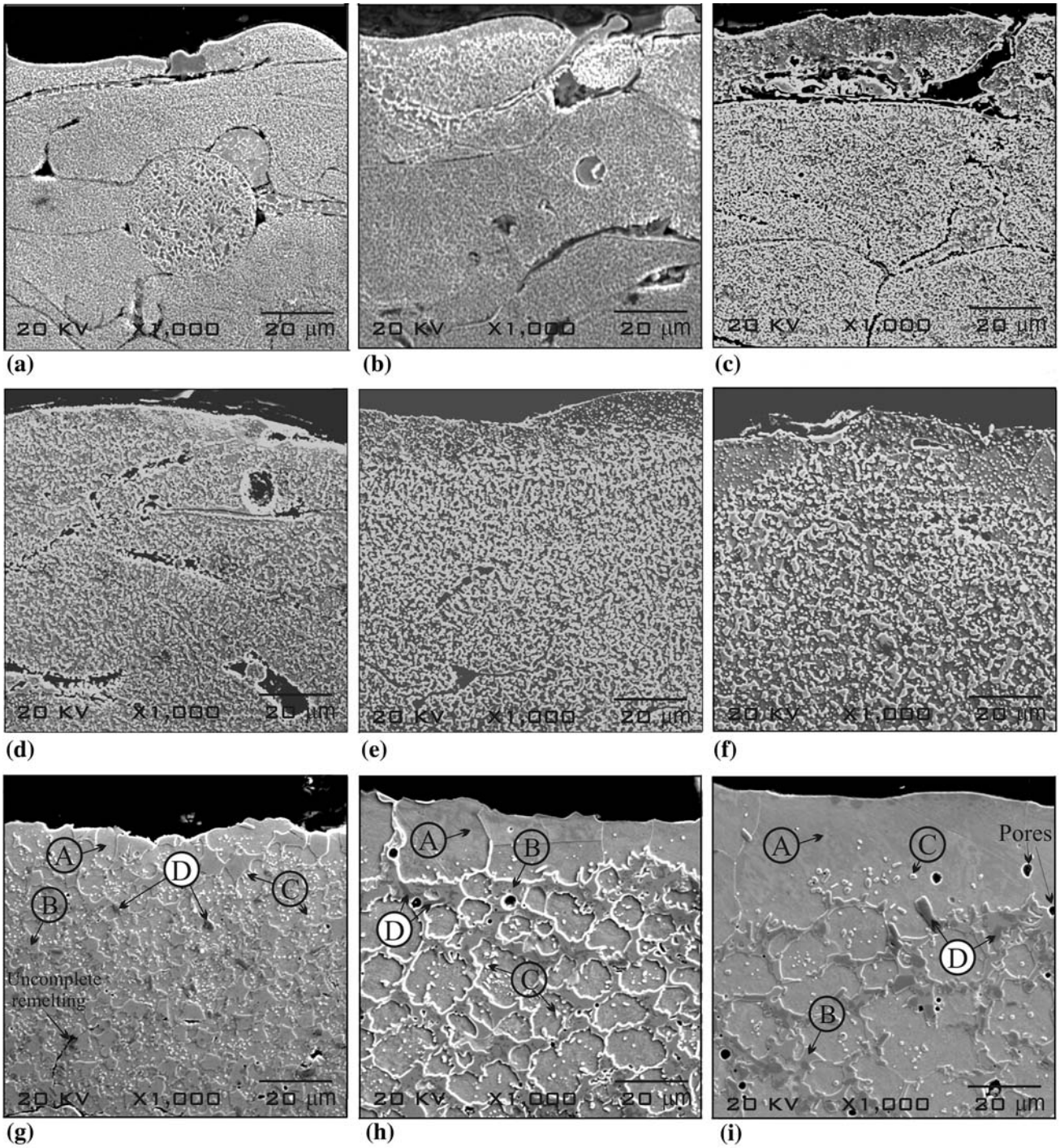

Fig. 6 Microstructure of NiCrBSi coatings at different temperature and time of postprocessing. (a) Heat treated at 930 °C, 5 min. (b) Heat treated at 930 °C, 10 min. (c) Heat treated at 930 °C, 20 min. (d) Heat treated at 1040 °C, 5 min. (e) Heat treated at 1040 °C, 10 min. (f) Heat treated at 1040 °C, 20 min. (g) Remelted at 1080 °C, 5 min. (h) Remelted at 1080 °C, 10 min. (i) Remelted at 1080 °C, 20 min

3.3.4 Measurement of Specimen Hardness. Through-depth microhardness measurements of the coating were made using the Vickers method, the load being 3 N on a Leitz Wetzlar gage (Leica Microsystems GmbH, Wetzlar, Germany). Figures 7(a) and (b) show a through-depth variation of microhardness to a depth of 700 μm of the as-sprayed coating and the substrate right after spraying and heat treatment, that is, remelting, of the coating. Results indicate that the highest coating microhardness is obtained in as-sprayed coatings. Reduction of microhardness of the NiCrBSi coating was also observed by Gonzales et al. (Ref 13) and Hyung et al. (Ref 17). It is a

result of a comparatively slower coating cooling after cooling in air than that of particle quenching during spraying, but it can also be a result of grain growth and phase transformations. Dissipation of microhardness results is attributed to microstructural heterogeneity in the coating and described by a standard deviation. The strongest dissipation of the microhardness values measured was found with coatings right after spraying. Relatively low hardness dissipation is beneficial, and it was found in the coating remelted at 1080 °C for 5 min. The substrate is of low-alloy steel with 0.08% C. It heats over the austenite temperature, which, in the process, produces desired diffusion bonds between the coating and the substrate. After heat treatment and remelting, the detrimental reduction of hardness and decarburizing of the substrate was also observed.

Figure 8 shows an average hardness value $\overline{HV}_{0.3}$ with the standard deviation. The histogram was constructed out of the hardness measurements, made at the constant depth below the surface. It was found that the average microhardness reduces with the duration of heat treatment of coatings heat-treated at 930 °C and remelted at 1080 °C. From Fig 8, an increasing trend of average microhardness is observed at temperature of 1040 °C. The possible reason for the increase of microhardness at that temperature could be the precipitation-hardening effect of the nickel alloys.

Table 5 Results of elemental chemical analysis, that is, energy-dispersive spectroscopy (EDS), for coatings, remelted at 1080 °C

Phase	Ni	Cr	Si	Fe
Fig. 6(g): remelted at 1080 °C, 5 min				
A	81.91	9.59	4.35	4.15
B	91.93	6.77	0.21	1.39
C	70.26	20.86	5.39	3.49
D	42.14	56.12	0.50	1.24
Area	76.16	15.18	4.06	4.59
Fig. 6 g: remelted at 1080 °C, 10 min				
A	82.32	9.67	4.10	3.91
B	88.40	8.11	0.39	3.18
C	63.19	32.10	2.96	3.33
D	11.82	84.33	0.47	2.01
Area	74.07	18.26	3.43	4.24
Fig. 6 g: remelted at 1080 °C, 20 min				
A	81.15	10.86	3.89	4.09
B	90.06	7.17	0.30	2.48
C	70.48	21.71	6.88	4.22
D	2.37	97.48	0.15	0
Area	75.24	17.08	3.52	4.16

3.3.5 Analysis of Porosity. In general, the porosity of a sprayed layer has a detrimental effect on the operating performance of the coating, unless the coating is used for bearings (Ref 1). The porosity was evaluated in the as-sprayed specimens as well as in those subjected to different heat treatment conditions. A Leitz Wetzlar microscope (Leica Microsystems Vertrieb GmbH, Wetzlar, Germany) under a 50× magnification and an Olympus Colorview camera (Tokyo, Japan) were used to observe porosity. Software package AnalysisDocu was used to process data on pore sizes and ImageTool for image processing. The porosity percentage [%] was obtained by measuring surface pores in a test field of 1000 by 400 μm in three fields of vision. Porosity measurements were

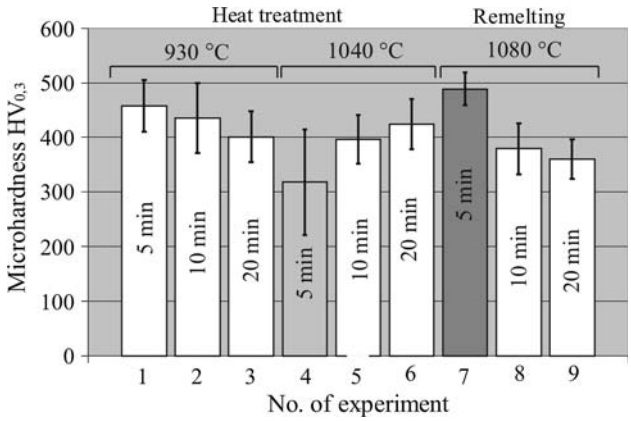

Fig. 8 Microhardness diagram for 9 combinations of heat treatment and remelting

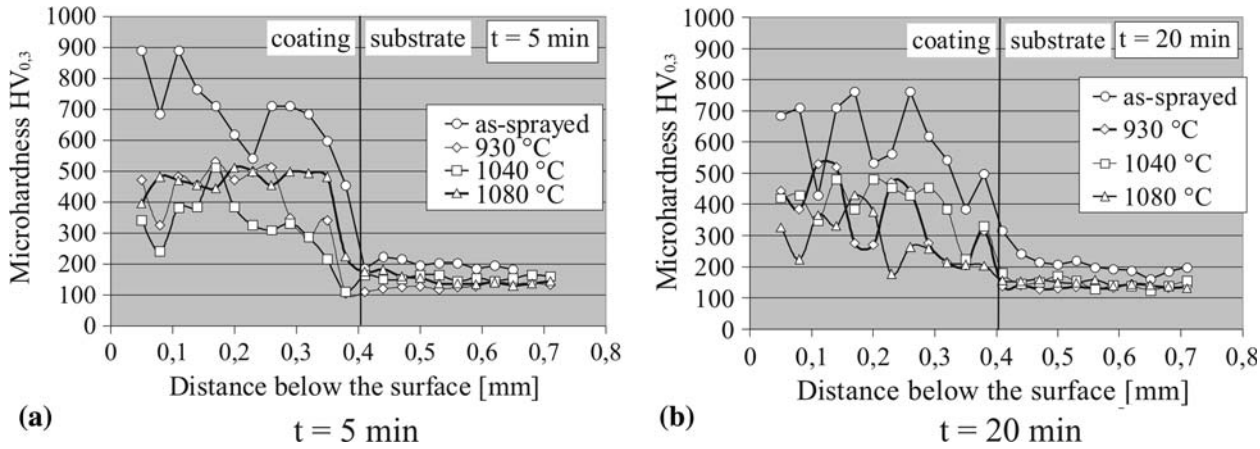

Fig. 7 Through-depth $HV_{0.3}$ microhardness variation of coating and substrate after heat treatment and remelting. (a) $t = 5$ min. (b) $t = 20$ min

made at a total of 27 fields of vision after deposition, and the same number of measurements was made after subsequent heat treatment and remelting. The average measured porosity for flame sprayed coating is approximately 10%. After heat treatment at 930 °C, the measured porosity percentage is between 2 and 3%; after heat treatment at 1040 °C the porosity is around 1%, as well as after remelting at 1080 °C. Figure 9 shows that the porosity percentage is inversely proportioned with the temperature of the thermal posttreatment. After heat treatment at 1040 °C, the lowest porosity is obtained after 10 and 20 min. In coatings that were furnace remelted at 1080 °C the pore fraction with the time intervals of 10 and 20 min of remelting increases as a result of release of gases during remelting and, consequently, formation of new pores in the coating.

3.3.6 Residual Stresses in Coatings. The analysis of residual stresses was performed in accordance with the standard method specified in ASTM E 837-08 (Ref 22). Residual stresses were determined with commercial measurement equipment, a product of Vishay Measurements Group (Vishay Intertechnology Inc., Malvern, PA, USA). The equipment makes it possible to determine residual stresses after the relaxation method where strain measurement is implemented during incremental drilling of a hole in a resistance measurement rosette located in the central part. A TiN coated milling-cutter with a diameter of 1.6 mm was chosen. On the basis of strains measured using a resistance rosette CEA-06-062UM-120, the size of two equivalent residual stress vectors, and their angle orientation with regard to the starting point set in accordance with the manufacturer's instructions are calculated. In the calculation of residual stresses, a modulus of elasticity of coatings was chosen, which is considerably lower than that of bulk-materials of the same chemical composition. Modulus of elasticity for nickel-based coatings, determined from Knoop microhardness test (Ref 15), was taken into account.

Figure 10(a) shows a residual-stress variation in the as-sprayed coating and substrate. The residual stresses increase in the tensile direction to the boundary between the coating and substrate, where the highest residual stress measured equals +387 MPa. Figure 10(b) shows a through-thickness residual-stress variation in the coating and substrate after 20 min remelting at 1080 °C. Surface stresses are relatively low, and at a depth of 0.1 mm one of stress components is even in a more favorable compressive range; that is, it is −64 MPa. The stresses pass to the tensile region and do not change as to their sign. In coatings, after remelting, the maximum component of an equivalent tensile residual stress reduces to +93 MPa, which is, from the viewpoint of resistance, much more favorable than in as-sprayed coating.

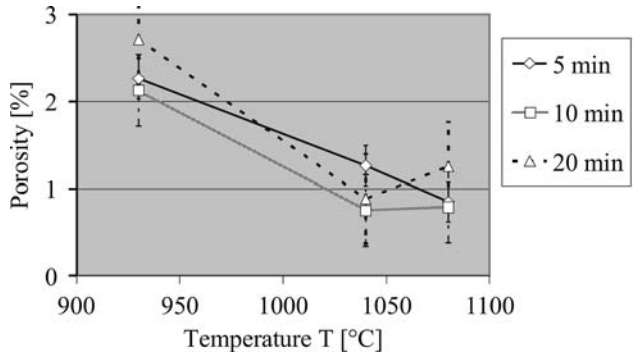

Fig. 9 Diagram of porosity reducement after heat treatment

4. Conclusions

Based on the investigation of two-step process deposition of NiCrBSi coating, flame spraying and subsequent furnace heat treatment and remelting, the following conclusions can be drawn:

- The matrix experiment under different conditions of substrate preparation and flame spraying confirmed that an improvement of the adhesion strength of flame sprayed coatings can be made using the Taguchi parametric method.
- After heat treatment at 930 °C, the failure of the adhesion/cohesion specimen assembly occurred

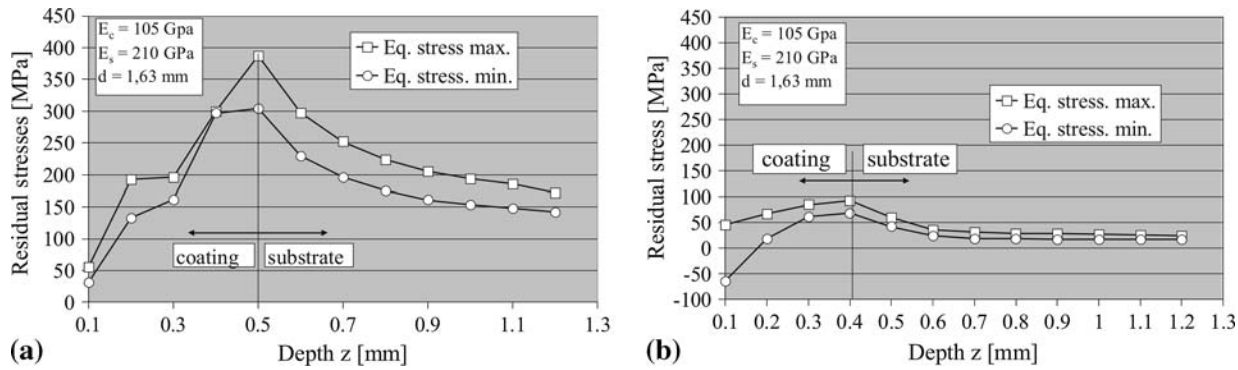

Fig. 10 Variation of equivalent residual stresses in as-sprayed coating and in coating after remelting. (a) After flame spray deposition. (b) Remelted at 1080 °C, 20 min

through the glued cross section. The final adhesion strength of coating is higher than the strength of the glue, which amounts to 50 MPa. In order to study the adhesion strength of heat treated coatings, another method should be used.

- Based on the metallographic analysis of the cross section of the as-sprayed coating, the two characteristic types of splats, regarding the shape and microstructure, are distinguished. The particles remelted in the flame have a nanoscale grained microstructure due to the rapid cooling at collision and an irregularly deformed shape, whereas unmelted splats are of a spheroidal shape and have a similar microstructure to the powder material prior to spraying.
- After heat treatment at 930 °C below the solidus line, the general morphology of coating was basically similar to as-sprayed coatings in all cases. A change is seen with slightly larger grain size. The presence of splat boundaries is still clearly visible.
- Lengthening of the heat treatment time at 1040 °C results in a gradual increase in grain size. At the same temperature and with 20 min heat treatment, diffusion processes will occur between particles (splat) interfaces, which shows in gradual disappearing of the splat boundaries.
- In melting at 1080 °C, almost complete fusion of the coating occurs in 5 min melting between the solidus and liquidus point of the alloy. The small and numerous inclusions, rich in chromium, are dissolving. They are, in the case of the 5 min remelting time, uniformly distributed in the coating microstructure. Lengthening of the melting time results in decreasing the number of precipitates in the thin surface layer of the coating. The chromium content and the size of blocky, larger, and less numerous darker precipitates gradually increase with time of furnace-melting.
- The as-sprayed coatings show the highest microhardness. This is a consequence of rapid cooling of splats at the cold surface during spraying. The softening occurs after heat treatment or remelting due to overtempering and slow cooling rates. At 1040 °C coating hardness increases with duration of heat treatment, possibly because of precipitation hardening. At 930 and 1080 °C, hardness is decreasing with duration of heat treatment, that is, remelting.
- As heat treatment and remelting is performed, the highest microhardness, that is, the one with an average value of 488 $HV_{0.3}$, was measured in the specimen coating remelted for 5 min at 1080 °C.
- From the analysis of porosity it is inferred that an important decrease of porosity fraction during remelting at 1080 °C for 5 min. After 10 and 20 min of remelting, however, new gas pores will occur.
- In the analysis of residual stresses it was found that tensile residual stresses after spraying reach the highest value at +387 MPa, whereas after remelting they reduce to +93 MPa.

The research findings show that the most suitable microstructure fusion is accomplished with 5 min remelting of the NiCrBSi coating. This provides a homogeneous microstructure with uniformly distributed chromium precipitates in the microstructure and low porosity. Reduction of tensile residual stresses provides better resistance and longer life of coatings in their operating environment.

References

1. J.R. Davis, *Handbook of Thermal Spray Technology*, ASM International, Materials Park, OH, 2004
2. M.H. Staia, E. Ramos, A. Carrasquero, A. Roman, J. Lesage, D. Chicot, and G. Mesmacque, Effect of Substrate Roughness Induced by Grit Blasting upon Adhesion of WC-17% Co Thermal Sprayed Coatings, *Thin Solid Films*, 2000, **377-378**, p 657-664
3. C.R.C. Lima and J.M. Guilemany, Adhesion Improvements of Thermal Barrier Coatings with HVOF Thermally Sprayed Bond Coats, *Surf. Coat. Technol.,* 2006. doi:10.1016/j.surfcoat.2006.0.05
4. H. Weiss, Adhesion of Advanced Overlay Coatings: Mechanisms and Quantitative Assessment, *Surf. Coat. Technol.*, 1995, **71**, p 201-207
5. M. Laribi, N. Mesrati, A.B. Vannes, and D. Treheux, Adhesion and Residual Stresses Determination of Thermally Sprayed Molybdenum on Steel, *Surf. Coat. Technol.*, 2003, **166**, p 206-212
6. "Standard Test Method for Adhesion or Cohesion Strength of Thermal Spray Coatings," C 633-01, *Annual Book of ASTM Standards,* Vol 02.05, ASTM International, West Conshohocken, PA, 2001
7. P. Fauchais, M. Fukumoto, A. Vardelle, and M. Vardelle, Knowledge Concerning Splat Formation: An Invited Review, *J. Thermal Spray Technol.*, 2003, **13**(3), p 337-359
8. R.S.C. Paredes, S.C. Amico, and A.S.C. d'Oliveira, The Effect of Roughness and Pre-heating of the Substrate on the Morphology of Aluminium Coatings Deposited by Thermal Spraying, *Surf. Coat. Technol.*, 2006, **200**, p 3049-3055
9. M. Vijaya Babu and R. Kumar, Fracture Mechanics Approaches to Coating Strength Evaluation, *Eng. Fract. Mech.*, 1996, **55**, p 235-248
10. W.-C. Lih, S.H. Yang, C.Y. Su, S.C. Hung, I.C. Hsu, and M.S. Leu, Effects of Process Parameters on Molten Particle Speed and Surface Temperature and the Properties of HVOS CrC NiCr Coatings, *Surf. Coat. Technol.*, 2000, **133-134**, p 54-60
11. J. Grum and J.M. Slabe, The Use of Factorial Design and Response Surface Methodology for Fast Determination of Optimal Heat Treatment Conditions of Different Ni-Co-Mo Surface Layers, *J. Mater. Process. Technol.*, 2004, **155-156**, p 2026-2032
12. M.S. Phadke, *Quality Engineering Using Robust Design*, Prentice-Hall Int. Inc, New Jersey, 1989
13. R. Gonzales, M.A. Garcia, I. Penuelas, M. Cadenas, Ma del Rocio Fernandez, A. Hernandez Battez, and D. Felgueroso, Microstructural Study of NiCrBSi Coatings Obtained by Different Processes, *Wear*, 2007, **263**, p 619-624
14. J. Grum and J.M. Slabe, Effect of Laser-Remelting of Surface Cracks on Microstructure and Residual Stresses in 12Ni Maraging Steel, *Appl. Surf. Sci.*, 2006, **252**, p 4486-4492
15. C. Godoy, E.A. Souza, M.M. Lima, and J.C.A. Batista, Correlation between Residual Stresses and Adhesion of Plasma Sprayed Coatings: Effects of a Post-Annealing Treatment, *Thin Solid Films*, 2002, **420-421**, p 438-445
16. S. Shrestha, A. Neville, and T. Hodgkiess, The Effect of Post-Treatment of a High-Velocity Oxy-Fuel Ni-Cr-Mo-Si-B Coating Part I: Microstructure/Corrosion Behaviour Relationships, *J. Therm. Spray Technol.*, 2001, **10**(3), p 470-479
17. H.-J. Kim, S.-Y. Hwang, C.-H. Lee, and P. Juvanon, Assessment of Wear Performance of Flame Sprayed and Fused Ni-Based Coatings, *Surf. Coat. Technol.*, 2003, **172**, p 262-269
18. D.C. Montgomery, *Design and Analysis of Experiments,* 5th ed., John Wiley & Sons, p 363-391

19. ''Produkt- und Anwendungs-Informationen,'' Castolin Eutectic GmbH, Wien, Austria, 2005 (in German)
20. *Alloy Phase Diagrams,* Vol 3, ASM Handbook, ASM International, p 83, 155, 318
21. ''Standard Guide for Metallographic Preparation of Thermal Sprayed Coatings,'' E 1920-03, Vol 03.01, *Annual Book of ASTM Standards,* ASTM International, West Conshohocken, PA, 2003
22. ''Standard Test Method for Determining Residual Stresses by the Hole-Drilling Strain-Gage Method,'' E 837-08, Vol 03.01, *Annual Book of ASTM Standards,* ASTM International, West Conshohocken, PA, 2008